JACS Au
AN OPEN ACCESS JOURNAL OF THE AMERICAN CHEMICAL SOCIETY

pubs.acs.org/jacsau
Letter

Structure Distortion Endows Copper Nanoclusters with Surface-Active Uncoordinated Sites for Boosting Catalysis

Jing Sun, Qingyuan Wu, Xiaodan Yan, Lei Li, Xiongkai Tang, Xuekun Gong, Bingzheng Yan, Qinghua Xu, Qingxiang Guo, Jinlu He,* and Hui Shen*

Cite This: JACS Au 2024, 4, 3427−3435

ABSTRACT: The utilization of structure distortion to modulate the electronic structure and alter catalytic properties of metallic nanomaterials is a well-established practice, but accurately identifying and comprehensively understanding these distortions present significant challenges. Ligand-stabilized metal nanoclusters with well-defined structures serve as exemplary model systems to illustrate the structure chemistry of nanomaterials, among which few studies have investigated nanocluster models that incorporate structural distortions. In this work, a novel copper hydride nanocluster, $Cu_{42}(PPh_3)_8(RS)_4(CF_3COO)_{10}(CH_3O)_4H_{10}$ (Cu_{42}; PPh_3 is triphenylphosphine and RSH is 2,4-dichlorophenylthiol), with a highly twisted structure has been synthesized in a simple way. Structural analysis reveals Cu_{42} comprises two Cu_{25} units that are conjoined in a nearly orthogonal manner. The dramatic distortion in the metal framework, which is driven by multiple interactions from the surface ligands, endows the cluster with a rich array of uncoordinated metal sites on the surface. The resulting cluster, as envisioned, exhibits remarkable activity in catalyzing carbonylation of anilines. The findings from this study not only provides atomically precise insights into the structural distortions that are pertinent to nanoparticle catalysts but also underscores the potential of structurally distorted NCs as a burgeoning generation of catalysts with precise structures and outstanding performances that can be tailored for specific functions.

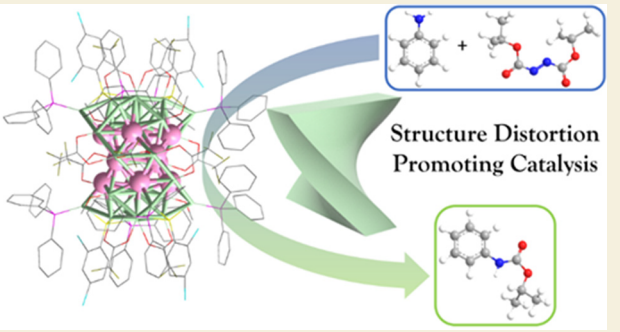

KEYWORDS: *copper, metal cluster, structure distortion, catalysts, surface reactivity*

Owing to their high specific surface area, metal nanoparticles have garnered great interest in the field of catalysis.[1] The catalytic properties of these nanoparticles are highly associated with surface active atoms that possess low coordination numbers in their structures.[2,3] Consequently, substantial efforts over the past decades have focused on tailoring the size, composition, shape, and surface/interface structure of metal nanoparticles, aiming at optimizing the quantity and modulating the local coordination environment of the exposed metal sites.[4−6] The creation of distorted structures is one of the most effective strategies to enhance catalytic activities of metal nanocatalysts, as such distortions frequently create high-energy active interfaces that facilitate the formation of surface-active uncoordinated sites.[7−9] For example, "surface distortion" is proposed to be pivotal in rationalizing the electrocatalytic properties of state-of-the-art of PtNi/C nanocatalysts, which feature distinctive compositions, shapes, sizes, and surface defects.[10] Given the complexity of structural distortion at the nanometer scale, which involves intricate atomic arrangements, electronic configurations, and spatial coordinates, it remains a formidable challenge to elucidate and engineer structurally distorted metal nanocatalysts with atomic level precision.

Together with complete monodispersion, well-defined compositions, and atomically precise structures, exceptional catalytic activity renders ligand-protected atomically precise metal nanoclusters (NCs) an ideal system to gain insight into structural distortions in metal nanocatalysts.[11−19] On one hand, the continuous advancements in determining molecular structures of numerous metal NCs, especially those composed of coinage metals (Au, Ag, and Cu), helps unravel the "holy grail" in nanocluster research.[20−32] For example, a family of metal frameworks including icosahedral, decahedral, and face-centered cubic structures has been extensively characterized. On the other hand, the structure configuration of metal NCs plays a crucial role in controlling the catalytic performances.[33−50] Our recent report demonstrated that copper NCs featuring an array-based geometry expose metal sites to a larger extent and thus promote catalysis.[51] Nevertheless, most of the

Received: July 1, 2024
Revised: August 3, 2024
Accepted: August 16, 2024
Published: August 22, 2024

https://doi.org/10.1021/jacsau.4c00574
JACS Au 2024, 4, 3427−3435

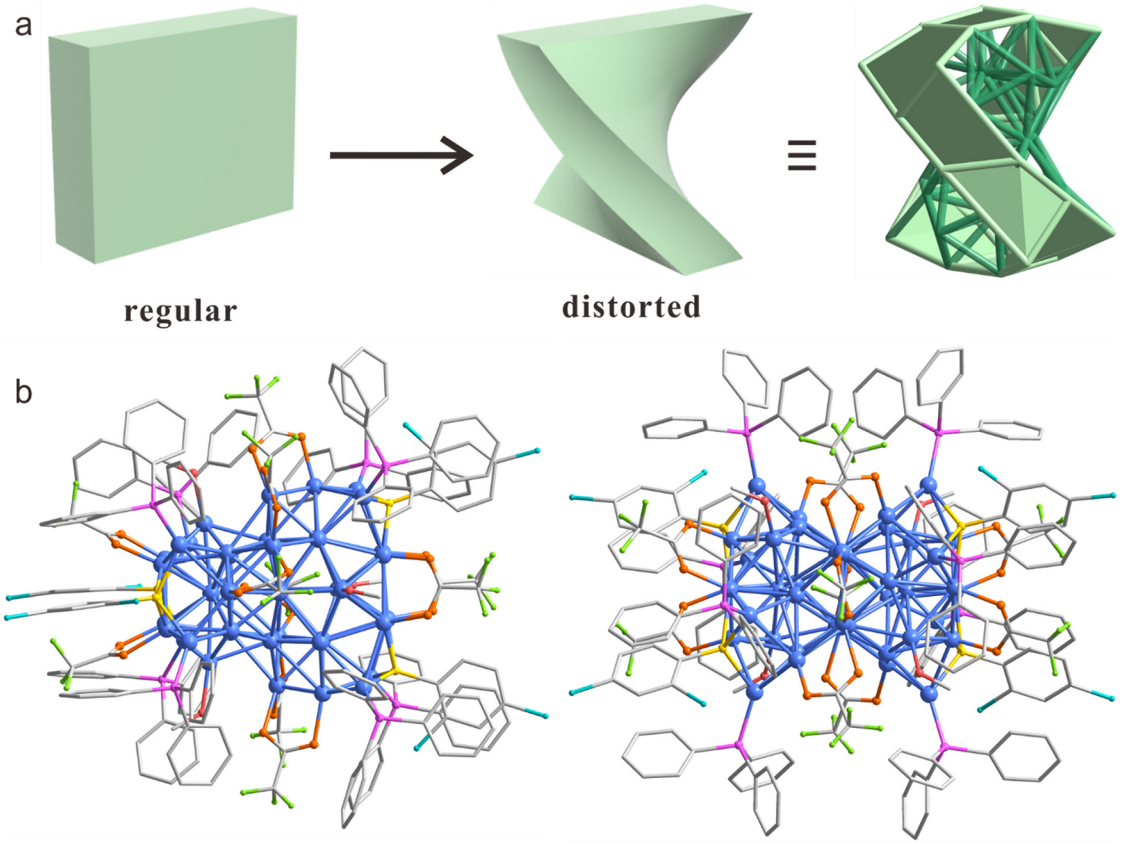

Figure 1. (a) Structural illustration of metal nanoclusters with regular and distorted structures. (b) Total structure of the $[Cu_{42}(PPh_3)_8(RS)_4(CF_3COO)_{10}(CH_3O)_4H_{10}]$ cluster. Color legend: Cu, blue; S, yellow; P, pink; Cl, turquoise; O, orange; F, bright green; C, gray. All hydrogen atoms are omitted for clarity.

metal NCs reported in the literature exist in regular geometries (Figure 1a), making the creation of those in highly distorted configurations a great challenge.[18] The principle of minimum energy forces the aggregation of metal atoms in NCs toward the equilibrium thermodynamic state, aiding in the stabilization of surface metal sites through protective ligands.[52] Of note, although Jin and co-workers have achieved structure distortion of Au_{24}(S-TBBM)$_{20}$ using a high-pressure strategy, its atomic structure in the distorted state remains undisclosed.[53]

Reported herein is the controlled synthesis, total structure determination, thorough characterization, and catalytic investigation of a highly distorted copper NC denoted as $Cu_{42}(PPh_3)_8(RS)_4(CF_3COO)_{10}(CH_3O)_4H_{10}$ (hereafter abbreviated as Cu_{42}), where PPh_3 is triphenylphosphine and RSH is 2,4-dichlorophenylthiol (Figure 1a). The cluster has been successfully fabricated by employing multiple kinds of ligands: while the bulky and rigid ligands (PPh_3 and RS^-) endow the structure with significant distortion, compact and flexible ligands (CF_3COO^- and CH_3O^-) help stabilize the structure. The metal framework of Cu_{42} consists of two Cu_{25} units that are fused in a surprisingly orthogonal way, thereby creating abundant uncoordinated sites on the boundary. As a result, it displays excellent performance in catalyzing carbonylation of anilines under mild reaction conditions.

The Cu_{42} cluster has been synthesized in one pot under ambient conditions (Scheme S1). The preparation of the cluster was initialized by bis(triphenylphosphino)-cuprous borohydride-mediated reduction of a mixture containing copper salt and thiol ligand in a solvent mixture of methanol and dichloromethane (for details see the Supporting Information). It gives rise to a dark red solution as the raw product, whose ultraviolet visible (UV−vis) spectrum confirms the formation of copper NCs (Figure S1). Subsequently, the formed clusters were then purified (by washing with H_2O) and crystallized (by diffusing ether into the cluster solution), leading to the growth of high-quality dark red crystals (Figure S2). Notably, the yield of crystalline products can be as high as 44.7% (based on Cu), which facilitates the follow-up investigations into the structure, characterization, and catalytic properties.

X-ray crystallographic analysis reveals that the Cu_{42} NC is in the monoclinic space group of $C2/c$ (Figure S3 and Table S1). In the lattice no counterion has been observed, indicating the neutral charge of the cluster (Figure S4). The cluster consists of 42 Cu atoms, 8 PPh_3 molecules, 4 RS^-, 10 CF_3COO^-, 4 MeO^-, and 10 hydride ligands, giving rise to the total formula $Cu_{42}(PPh_3)_8(RS)_4(CF_3COO)_{10}(CH_3O)_4H_{10}$ (note: the precise number of hydride atoms in the cluster was determined using electrospray ionization mass spectrometry (ESI-MS; *vide infra*)). Figure 1b shows the total structure of Cu_{42}, which describes the stabilization of a Cu_{42} core by an organic shell. The cluster has an overall length of 22.772 Å, as shown in Figure S5.

Constructed from the merging of two identical Cu_{25} units, the metal framework of Cu_{42} is highly distorted. As displayed in Figure 2a, each Cu_{25} unit originates from a centered Cu_{13} icosahedron with Cu−Cu bond lengths between the Cu center

https://doi.org/10.1021/jacsau.4c00574
JACS Au 2024, 4, 3427−3435

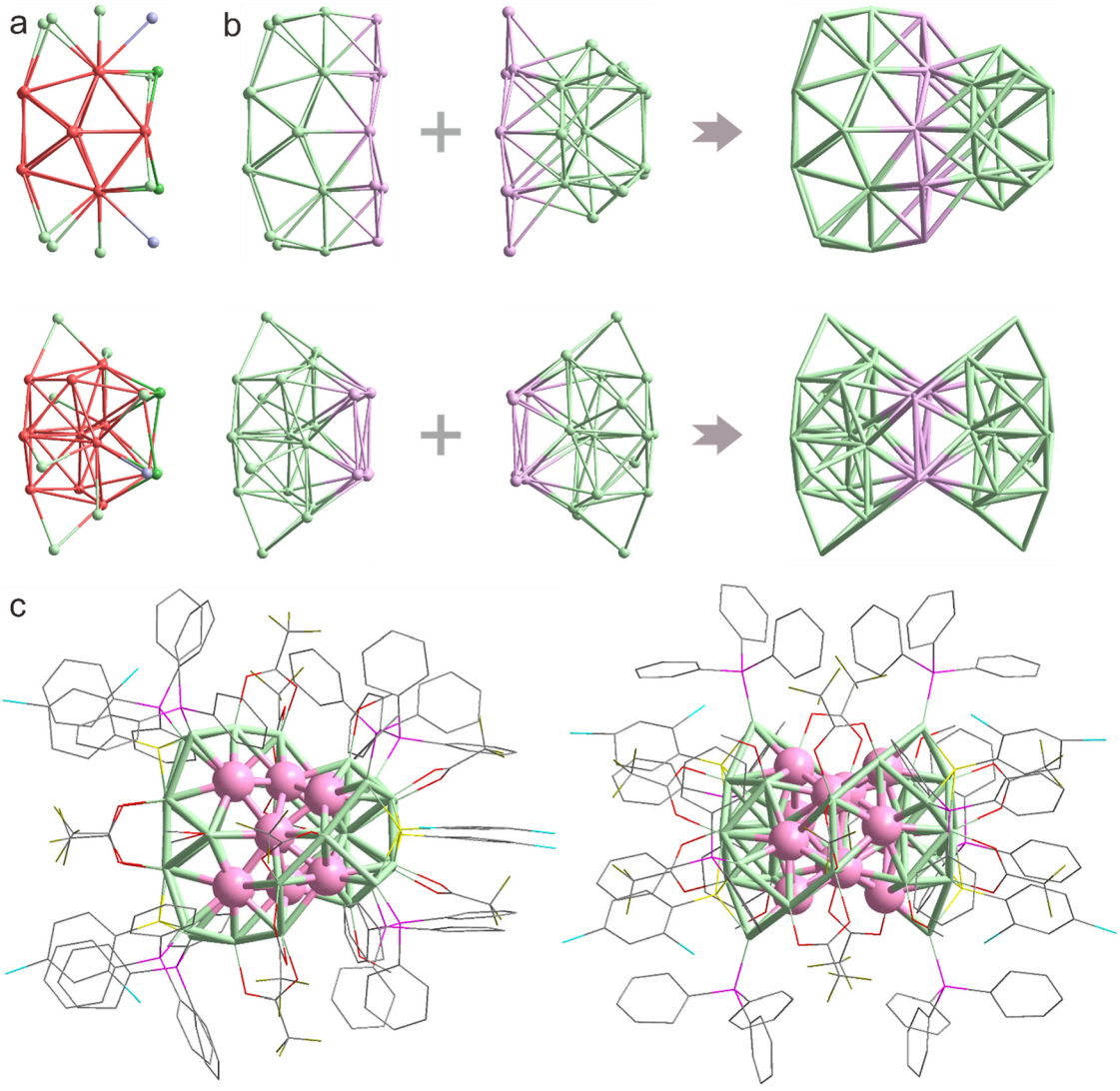

Figure 2. Structural anatomy of the Cu_{42} cluster. (a) Cu_{25} core. (b) Fusion of two Cu_{25} units to form the total metal framework of the Cu_{42} cluster. (c) The presence of rich surface-active uncoordinated sites (marked as pale pink) in the cluster. Color legend: Cu, red, pale green, and pale pink; S, yellow; P, dark pink; Cl, turquoise; O, red; F, dark yellow; C, gray. All other atoms are omitted for clarity.

and the surrounding Cu_{12} shell in the range of 2.5931−3.0683 Å, comparable to those found in $[Cu_{29}(AdmS)_{12}(PPh_3)_4Cl_6H_{10}]^+$ (Cu_{29}).[54] The bond distances of Cu−Cu in the Cu_{12} cage lie in the range of 2.4887−3.0957 Å. Surrounding the Cu_{13} icosahedron are 12 additional Cu atoms, with 8 at the vertices, 2 capping the Cu_4 faces, and the remaining 2 extending outward (Figure S6). Of particular interest, the geometric structure of Cu_{42} is characterized by an unexpected fusion of two Cu_{25} units, sharing an 8-copper face in a ladder shape (Figure S7). Nevertheless, these two identical Cu_{25} units are oriented in nearly orthogonal directions, making the overall framework highly twisted and deflected out of the regular shape (Figure 2b). Notably, no such high distortion has been observed in previously reported 42-atom metal NCs (Figure S8).[55,56]

Interestingly, the highly distorted arrangement of the two Cu_{25} units endows the Cu_{42} cluster with an abundance of surface uncoordinated metal sites (Figure 2c). The surface uncoordinated coverage of the cluster can reach up to 30% (defined as the ratio of the number of uncoordinated copper atoms on the surface to the number of all copper atoms on the surface). The distortion and the conquensequent presence of surface uncoordinated sites are attributed to the introduction of bulky and rigid ligands of 2,4-dichlorophenylthiol and triphenylphosphine. As is well-documented in the literature, the van der Waals repulsion between bulky ligands would leave the surface metal atoms between ligands uncoordinated.[4,42,57] Moreover, rigid ligands restrict the free motion of neighboring ligands, thus again intensifying the distortion of the metal architecture. Besides that, some other compact and flexible ligands (CF_3COO^- and CH_3O^-) help stabilize the cluster structure, ensuring its robustness in air (Figure S9). Further details of coordination modes and bond lengths of the ligands on the cluster can be found in Figure S10 and Tables S2 and S3.

The high-yield synthetic prototype allows for comprehensive characterization of the cluster by other advanced techniques. Despite being a charge-neutral cluster, distinguishable peaks in the 2800−2870 m/z range are observed in its ESI-MS in the positive mode. As illustrated in Figure 3a, these peaks are separated by m/z = 0.5, indicating a charge of +2. After considering all possibilities, the prominent peak at 2815.27 $m/$

https://doi.org/10.1021/jacsau.4c00574
JACS Au 2024, 4, 3427−3435

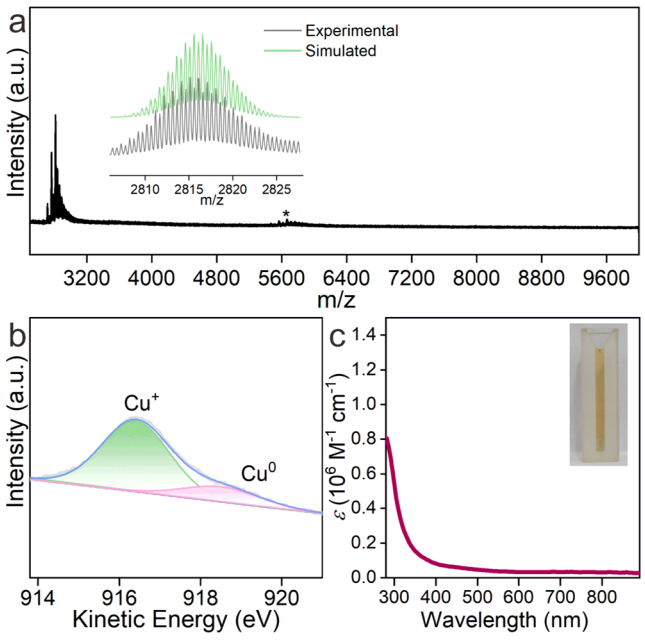

Figure 3. (a) HRESI-MS of Cu_{42} in the positive mode. The inset is a comparison between experimental (gray trace) and simulated (green trace) isotopic patterns of the molecular peak of $[Cu_{42}(PPh_3)_5(RS)_2(CF_3COO)_{10}(CH_3O)_4H_{10}(CH_3OH)]^{2+}$. Note: the peak marked with an asterisk corresponds to $[Cu_{41}(PPh_3)_5(RS)_4(CF_3COO)_8(CH_3O)_4H_{10}]^+$. (b) Cu LMM X-ray-excited Auger electron spectroscopy of Cu_{42}. (c) UV−vis spectrum of the Cu_{42} cluster in DCM (dichloromethane). The inset is a photograph of the cluster solution in DCM.

z is finally assigned to be $[Cu_{42}(PPh_3)_5(RS)_2(CF_3COO)_{10}(CH_3O)_4H_{10}(CH_3OH)]^{2+}$ (calcd 2815.2 m/z). Other peaks correspond to the fragments containing a tunable number of surface ligands (Figure S11). To verify the presence of 10 hydride atoms in the cluster, the deuterated analogues Cu_{42}-D were prepared and analyzed by ESI-MS. As shown in Figure S12, the calculated isotopic patterns match the experimental ones, confirming the composition and revealing that Cu_{42} contains 10 hydride atoms: namely, the number of free valence electrons in the cluster is 14. To the best of our knowledge, Cu_{42} is the first copper-hydride metal NC with 14 free electrons.[11,58,59] The above results also suggest that both Cu^0 and Cu^I atoms are present in the cluster. X-ray photoelectron spectroscopy (XPS) was used to investigate the Cu oxidation state. As shown in Figure S13, two binding energy peaks at 932 and 952 eV are observed in the XPS spectrum of Cu_{42}, which are attributed to the Cu $2p_{3/2}$ and Cu $2p_{1/2}$ orbitals, respectively. The absence of large oscillatory satellite peaks between 938 and 946 eV suggests the absence of Cu^{2+} species in the product.[60] Notably, it is often challenging to distinguish Cu^0 and Cu^+ from the XPS studies, as the difference between their binding energies is small (0.1 eV).[61] To further draw a convincing conclusion, we have carefully analyzed the Cu LMM Auger spectrum of the cluster. The peaks are deconvoluted into two peaks of Cu^+ and Cu^0 species using the XPSPEAK41 software. The peaks at 916.4 and 918.3 eV in the Cu LMM Auger spectrum confirm that both Cu^+ and Cu^0 are present in Cu_{42} (Figure 3b).[62] Additionally, the cluster samples were characterized by scanning electron microscopy (SEM) coupled with energy-dispersive X-ray spectroscopy (EDS). As illustrated in Figure S14, EDS elemental mappings confirm the presence of Cu, O, P, Cl, S, F, and C in the Cu_{42} NC. As shown in Figure 3c, the cluster sample appears yellow in dichloromethane (DCM) and exhibits a strong absorption peak at 280 nm in its UV−vis spectrum.

We also endeavored to delineate the positions of the 10 hydride atoms within the Cu_{42} cluster. By meticulously examining the crystal structure and leveraging the data from previously characterized copper-hydride clusters, we inferred the locations of the hydrides from residual peaks in the difference electron density map derived from crystallographic data. The precise coordinates of these hydrides were subsequently refined using least-squares methods.[24,63−65] To deepen our understanding of the structure and stability of these hydride-containing configurations, density functional theory (DFT) calculations (further details provided below) were conducted. Considering the C_2 symmetry of the Cu_{42} cluster, only a half-representation of the structure is depicted herein for clarity. As delineated in Figure S15a,b, the hydrides housed within the Cu_{42} cluster are categorized into four discernible types based on their coordination modes and spatial positions. The primary type of hydride atoms (type 1, depicted in blue in Figure S15c) is nestled within the structure, coordinated by four Cu atoms in a configuration reminiscent of a butterfly motif. The Cu−H bond lengths in the mode are averaged to be 1.753 Å. Conversely, the remaining types of hydride atoms are situated on the surface of the Cu_{42} core, adopting triangular-pyramidal (type 2, depicted in pink in Figure S15d), triangular-bipyramidal (type 3, orange in Figure S15e), or square-pyramidal (type 4, sky blue in Figure S15f) geometries. The average Cu−H distances for these three types of hydride locations were determined to be 1.890 Å (type 2), 1.889 Å (type 3), and 1.833 Å (type 4), respectively, which are comparable to those observed in $[Cu_{25}H_{10}(SPhCl_2)_{18}]^{3-}$ and $[Cu_{23}(PhSe)_{16}(Ph_3P)_8H_6]^+$.[36,66]

DFT computations were then utilized to delve into the electronic structure of the cluster and to authenticate the rationality of the hydride atoms' position in the structure. Commencing from the crystal structure, the geometry optimization and electronic structure analysis of the Cu_{42} cluster were performed using the Gaussian 09 program (see technical details in the Supporting Information). Figure 4 displays the charge density distributions of the frontier orbitals and the partial density of states (PDOS) of the Cu_{42} cluster. As depicted in Figure 4a, the charge densities of the highest occupied molecular orbital (HOMO) and the lowest unoccupied molecular orbital (LUMO) states predominantly originate from the Cu atoms which are located inside the Cu_{42} cluster. Minor contributions from other elements (such as P and S) were observed near the band edge states, aligning well with the partial density of states (PDOS) in Figure 4b. The computational estimation of the energy gap between the HOMO and LUMO states yielded a value of 1.46 eV (Figure 4b and Table S4), suggesting a high stability of the cluster in terms of electronic structure. The optimized fractional atomic coordinates and calculated bond lengths are given in Tables S5 and S6. Moreover, the important calculated interatomic distances agree well with the experimental values, thereby affirming the validity of the employed structure (Table S7).

The presence of unsaturated coordination sites on the surfaces of the clusters is further confirmed quantitatively through luminescent titration using the probe molecule aniline. This approach has previously been utilized to quantitatively

https://doi.org/10.1021/jacsau.4c00574
JACS Au 2024, 4, 3427−3435

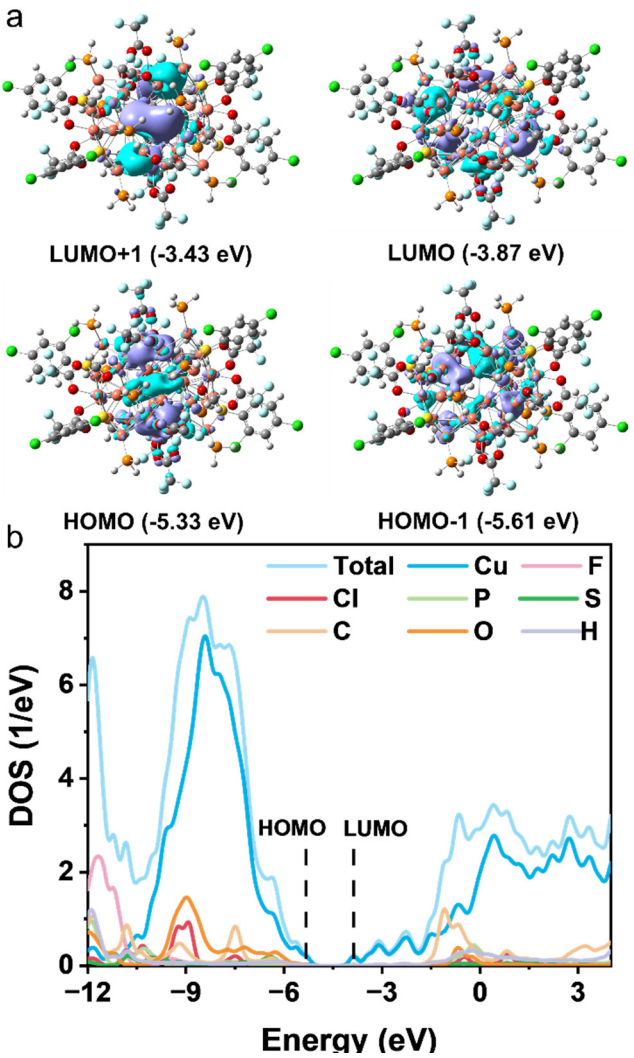

Figure 4. (a) Frontier orbitals including LUMO+1, LUMO, HOMO, and HOMO-1 for the Cu_{42} cluster. (b) Partial density of states (PDOS) of the cluster.

assess the accessible area of metal clusters.[57,67,68] Aniline exhibits fluorescence in solution, which is diminished when it chemisorbs onto the cluster surface. As depicted in Figure S16a, the fluorescence of the aniline solution was promptly quenched upon the addition of an equivalent Cu_{42} cluster. A significant decrease in fluorescence signifies the successful chemisorption of the molecules onto the copper sites of the surface. The fluorescence intensity remained nearly constant upon the addition of more aniline until approximately 9 equiv of aniline was added. As additional aniline was introduced, the emission exhibited a linear increase with the amount of aniline (Figure S16b). The luminescence of the excess free aniline can be observed because the 9 uncoordinated sites have been occupied. The titration results provide insight into the accessibility of the nine uncoordinated sites of Cu_{42}.

Because of the large number of unsaturated coordination sites on its surface and moderate stability, it occurs to us that Cu_{42} emerges as a promising candidate for catalytic applications. In the pursuit of efficient methods for the direct synthesis of carbamate compounds through the formation of C−N bonds using copper catalysis, we selected the carbonylation of anilines as a model reaction.[69,70] We initially optimized the reaction conditions of aniline **1a** with diisopropyl azodicarboxylate **2** using Cu_{42} as the catalyst. Encouragingly, the cluster is able to catalyze the reaction at room temperature, affording the desired product of carbamate **3a** in ≥99% yield after 3 h (Table 1, entry 1). The pivotal role

Table 1. Carbonylation of Anilines by Various Catalysts[a]

entry	catalyst	yield[b] (%)
1	Cu_{42}	>99
2[c]	Cu_{29}	10
3[c]	Cu_{14}	30
4[c]	CuI	24
5[c]	$Cu(CF_3COO)_2$	33

[a]Reaction conditions: **1** a (0.6 mmol), **2** (1.2 mmol), and Cu_{42}/XC-72 (0.1 mmol % based on cluster) in $CDCl_3$ (1 mL) in air at room temperature for 3 h. [b]Yields were determined by ^1H NMR with 1,3,5-trimethoxybenzene as internal standard. [c]The amount of Cu atoms in each catalyst was kept the same.

of surface-active uncoordinated sites in driving the catalytic conversion was highlighted, as evidenced by significantly lower yields for the corresponding product obtained when using alternative reported clusters (Cu_{29} and $Cu_{14}(RCOO)_6(AdmS)_8(Cu_{14})$) as catalysts (Table 1, entries 2 and 3). It is worth noting that the products were observed in much lower yields when Cu complexes (such as CuI and $Cu(CF_3COO)_2$) were employed (Table 1, entries 4 and 5), reaffirming the superior catalytic activity of the cluster species.

After optimizing the reaction conditions, an extensive analysis of this Cu_{42}-catalyzed carbonylation of aniline reactions was conducted to ascertain the scope of this catalytic process. This catalytic reaction proved the remarkable versatility of this catalytic system, as it exhibited tolerance toward a diverse array of amines, facilitating the generation of carbamates featuring tailored structures and functional groups. Specifically, anilines whose para substituents on the aryl ring were substituted by either electron-donating (Me and OMe) or electron-withdrawing (F, Br, and formyl group) groups, underwent efficient conversion to their respective products with high yields (Table 2, entries 2−10, 13, and 15). Even when 2,4-dimethylaniline and 3,4-dimethylaniline, which may display large steric hindrance, were used as the reactants, the products **3k and 3l** were given in moderate yield (Table 2, entries 11 and 12). When aromatic heterocyclic aniline **1n** was employed, the corresponding product **3n** was also obtained in an excellent yield (Table 2, entry 14). Meanwhile, XPS and transmission electron microscopy (TEM) analysis of the catalysts highlight the robust capability before and after the catalytic reaction (Figures S17 and S18). Overall, this Cu_{42} catalyst represents promise in accommodating a variety of carbamate compounds via the direct C−N coupling between amines and azodicarboxylates.

In summary, a structurally distorted $Cu_{42}(PPh_3)_8(RS)_4(CF_3COO)_{10}(CH_3O)_4H_{10}$ (Cu_{42}) nanocluster has been obtained in high yield and its structure has been totally determined. The metal architecture of the cluster is made up of two identical Cu_{25} units that align orthogonally. The multiple ligands on its surface serve to rationalize the formation of the Cu_{42} cluster: while the bulky and rigid ones induce the distortion of the cluster backbone, those that are compact and flexible enhance its stability. Notably, the pronounced structure distortion of the cluster creates a large

https://doi.org/10.1021/jacsau.4c00574
JACS Au 2024, 4, 3427−3435

Table 2. Cu_{42} NC Catalysis of the Carbonylation of Anilines[a]

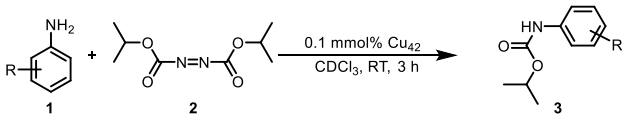

Entry	Substrate	Product	Yield[b] (%)
1	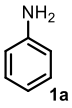	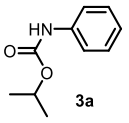	>99
2	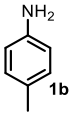	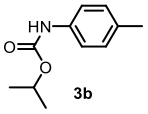	93
3		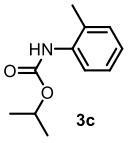	74
4	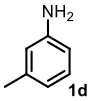	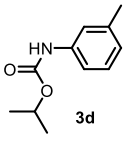	>99
5	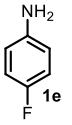	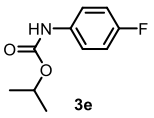	>99
6[c]	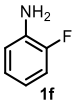	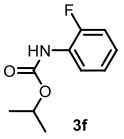	88
7[c]	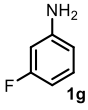	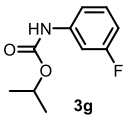	>99
8[c]	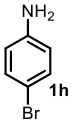	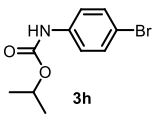	73
9[c]	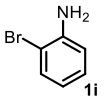	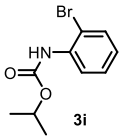	>99
10[c]	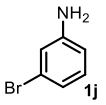	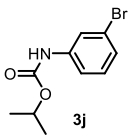	89
11[c]	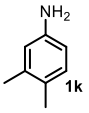	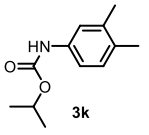	>99
12	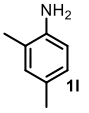	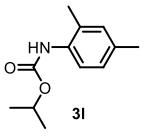	80
13[c]	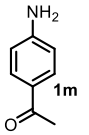	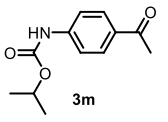	68
14[c]	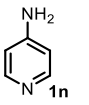	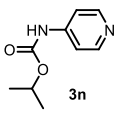	>99
15	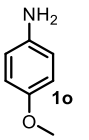	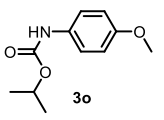	69

[a]Reaction conditions unless stated otherwise: anilines **1** (0.6 mmol), **2** (1.2 mmol), and 0.1 mmol % Cu_{42} catalyst (10 wt % loading with XC/72) in $CDCl_3$ (1 mL) under atmosphere at room temperature for 3 h. [b]Yields were determined by ^1H NMR with 1,3,5-trimethoxybenzene as internal standard. [c]The reaction time was 8 h under standard reaction conditions.

amount of uncoordinated metal sites on its surface, rendering it an effective catalyst for the carbonylation of anilines under mild conditions. The controlled synthesis and detailed studies of structurally distorted nanoclusters not only deepen our understanding of structure distortion chemistry that is significant in nanoparticulate catalysts but also fuel further exploration into the underlying principles that may transcend catalysis and find applications in diverse scientific domains.

■ ASSOCIATED CONTENT

Supporting Information

The Supporting Information is available free of charge at https://pubs.acs.org/doi/10.1021/jacsau.4c00574.

Crystallographic data (CIF)

Experimental details, digital photographs, crystal structure, stability evaluation, XPS, and TEM, and crystallographic data (PDF)

https://doi.org/10.1021/jacsau.4c00574
JACS Au 2024, 4, 3427−3435

AUTHOR INFORMATION

Corresponding Authors

Hui Shen − *College of Energy Materials and Chemistry, Inner Mongolia University, Hohhot 010021, People's Republic of China;* orcid.org/0000-0003-4800-437X; Email: shen@imu.edu.cn

Jinlu He − *College of Chemistry and Chemical Engineering, Inner Mongolia University, Hohhot 010021, People's Republic of China;* orcid.org/0000-0001-9772-8572; Email: hejinlu@imu.edu.cn

Authors

Jing Sun − *College of Energy Materials and Chemistry, Inner Mongolia University, Hohhot 010021, People's Republic of China*

Qingyuan Wu − *State Key Laboratory for Physical Chemistry of Solid Surfaces, College of Chemistry and Chemical Engineering, Xiamen University, Xiamen 361005, People's Republic of China*

Xiaodan Yan − *College of Chemistry and Chemical Engineering, Inner Mongolia University, Hohhot 010021, People's Republic of China*

Lei Li − *State Key Laboratory for Physical Chemistry of Solid Surfaces, College of Chemistry and Chemical Engineering, Xiamen University, Xiamen 361005, People's Republic of China*

Xiongkai Tang − *State Key Laboratory for Physical Chemistry of Solid Surfaces, College of Chemistry and Chemical Engineering, Xiamen University, Xiamen 361005, People's Republic of China*

Xuekun Gong − *College of Energy Materials and Chemistry, Inner Mongolia University, Hohhot 010021, People's Republic of China*

Bingzheng Yan − *College of Energy Materials and Chemistry, Inner Mongolia University, Hohhot 010021, People's Republic of China*

Qinghua Xu − *College of Energy Materials and Chemistry, Inner Mongolia University, Hohhot 010021, People's Republic of China;* orcid.org/0009-0009-8638-4474

Qingxiang Guo − *College of Chemical Engineering, Inner Mongolia University of Technology, Hohhot 010051, People's Republic of China;* orcid.org/0000-0001-7391-2893

Complete contact information is available at: https://pubs.acs.org/10.1021/jacsau.4c00574

Author Contributions

J.S., Q.W., and X.Y. contributed equally to this work.

Notes

The authors declare no competing financial interest.

ACKNOWLEDGMENTS

H.S. acknowledges financial support from the National Key R&D Program of China (2023YFB3507100), the National Natural Science Foundation of China (22301149), the Program for Young Talents of Science and Technology in Universities of Inner Mongolia Autonomous Region (NJYT23035), and start-up funding of Inner Mongolia University (10000-23112101/043). H.S. expresses his greatest appreciation to Professor Nanfeng Zheng (Xiamen University) for his generous support.

REFERENCES

(1) Xie, C.; Niu, Z.; Kim, D.; Li, M.; Yang, P. Surface and Interface Control in Nanoparticle Catalysis. *Chem. Rev.* **2020**, *120*, 1184−1249.

(2) Xu, Y.; Li, F.; Xu, A.; Edwards, J.; Hung, S.; Gabardo, C.; O'Brien, C.; Liu, S.; Wang, X.; Li, Y.; Wicks, J.; Miao, R.; Liu, Y.; Li, J.; Huang, J.; Abed, J.; Wang, Y.; Sargent, E. H.; Sinton, D. Low coordination number copper catalysts for electrochemical CO_2 methanation in a membrane electrode assembly. *Nat. Commun.* **2021**, *12*, 2932.

(3) Pan, H.; Dshemuchadse, J. Targeted Discovery of Low-Coordinated Crystal Structures via Tunable Particle Interactions. *ACS Nano* **2023**, *17*, 7157−7169.

(4) Jing, W.; Shen, H.; Qin, R.; Wu, Q.; Liu, K.; Zheng, N. F. Surface and Interface Coordination Chemistry Learned from Model Heterogeneous Metal Nanocatalysts: From Atomically Dispersed Catalysts to Atomically Precise Clusters. *Chem. Rev.* **2023**, *123*, 5948−6002.

(5) Liu, P. X.; Qin, R. X.; Fu, G.; Zheng, N. F. Surface Coordination Chemistry of Metal Nanomaterials. *J. Am. Chem. Soc.* **2017**, *139*, 2122−2131.

(6) Boles, M. A.; Ling, D.; Hyeon, T.; Talapin, D. V. The surface science of nanocrystals. *Nat. Mater.* **2016**, *15*, 141−153.

(7) Liu, J.; Zhang, J. Nanointerface Chemistry: Lattice-Mismatch-Directed Synthesis and Application of Hybrid Nanocrystals. *Chem. Rev.* **2020**, *120*, 2123−2170.

(8) Xia, Z.; Guo, S. Strain engineering of metal-based nanomaterials for energy electrocatalysis. *Chem. Soc. Rev.* **2019**, *48*, 3265−3278.

(9) Wu, G.; Han, X.; Cai, J.; Yin, P.; Cui, P.; Zheng, X.; Li, H.; Chen, C.; Wang, G.; Hong, X. In-plane strain engineering in ultrathin noble metal nanosheets boosts the intrinsic electrocatalytic hydrogen evolution activity. *Nat. Commun.* **2022**, *13*, 4200.

(10) Chattot, R.; Le Bacq, O.; Beermann, V.; Kühl, S.; Herranz, J.; Henning, S.; Kühn, L.; Asset, T.; Guétaz, L.; Renou, G.; Drnec, J.; Bordet, P.; Pasturel, A.; Eychmüller, A.; Schmidt, T.; Strasser, P.; Dubau, L.; Maillard, F. Surface distortion as a unifying concept and descriptor in oxygen reduction reaction electrocatalysis. *Nat. Mater.* **2018**, *17*, 827−833.

(11) Dhayal, R. S.; van Zyl, W. E.; Liu, C. W. Polyhydrido Copper Clusters: Synthetic Advances, Structural Diversity, and Nanocluster-to-Nanoparticle Conversion. *Acc. Chem. Res.* **2016**, *49*, 86−95.

(12) Ghosh, A.; Mohammed, O. F.; Bakr, O. M. Atomic-Level Doping of Metal Clusters. *Acc. Chem. Res.* **2018**, *51*, 3094−3103.

(13) Konishi, K.; Iwasaki, M.; Shichibu, Y. Phosphine-Ligated Gold Clusters with Core+exo Geometries: Unique Properties and Interactions at the Ligand-Cluster Interface. *Acc. Chem. Res.* **2018**, *51*, 3125−3133.

(14) Tang, Q.; Hu, G.; Fung, V.; Jiang, D. Insights into Interfaces, Stability, Electronic Properties, and Catalytic Activities of Atomically Precise Metal Nanoclusters from First Principles. *Acc. Chem. Res.* **2018**, *51*, 2793−2802.

(15) Yao, Q.; Chen, T.; Yuan, X.; Xie, J. Toward Total Synthesis of Thiolate-Protected Metal Nanoclusters. *Acc. Chem. Res.* **2018**, *51*, 1338−1348.

(16) Chakraborty, I.; Pradeep, T. Atomically Precise Clusters of Noble Metals: Emerging Link between Atoms and Nanoparticles. *Chem. Rev.* **2017**, *117*, 8208−8271.

(17) Du, Y.; Sheng, H.; Astruc, D.; Zhu, M. Atomically Precise Noble Metal Nanoclusters as Efficient Catalysts: A Bridge between Structure and Properties. *Chem. Rev.* **2020**, *120*, 526−622.

(18) Jin, R.; Zeng, C.; Zhou, M.; Chen, Y. Atomically Precise Colloidal Metal Nanoclusters and Nanoparticles: Fundamentals and Opportunities. *Chem. Rev.* **2016**, *116*, 10346−10413.

(19) Matus, M.; Häkkinen, H. Understanding ligand-protected noble metal nanoclusters at work. *Nat. Rev. Mater.* **2023**, *8*, 372−389.

(20) Ghosh, A.; Huang, R. W.; Alamer, B.; Abou-Hamad, E.; Hedhili, M. N.; Mohammed, O. F.; Bakr, O. M. $[Cu_{61}(S^tBu)_{26}S_6Cl_6H_{14}]^+$: A Core-Shell Superatom Nanocluster with a Quasi-J36 Cu_{19} Core and an "18-Crown-6" Metal-Sulfide-like Stabilizing Belt. *ACS Mater. Lett.* **2019**, *1*, 297−302.

(21) Luo, P.; Bai, S.; Wang, X.; Zhao, J.; Yan, Z. N.; Han, Y. F.; Zang, S. Q.; Mak, T. C. W. Tuning the Magic Sizes and Optical Properties of Atomically Precise Bidentate N-Heterocyclic Carbene-Protected Gold Nanoclusters via Subtle Change of N-Substituents. *Adv. Opt. Mater.* **2021**, *9*, 2001936.
(22) Chen, S.; Du, W.; Qin, C.; Liu, D.; Tang, L.; Liu, Y.; Wang, S.; Zhu, M. A New Approach to Assemble the Thiolated $[Au_1Ag_{22}(S\text{-}Adm)_{12}]^{3+}$ Superatom Complex into a Framework Material: Directly Linked by SbF_6^- Anions. *Angew. Chem., Int. Ed.* **2020**, *59*, 7542−7547.
(23) Han, X.; Luan, X.; Su, H.; Li, J.; Yuan, S.; Lei, Z.; Pei, Y.; Wang, Q. M. Structure Determination of Alkynyl-Protected Gold Nanocluster $Au_{22}(^tBuC{\equiv}C)_{18}$ and Its Thermochromic Luminescence. *Angew. Chem., Int. Ed.* **2020**, *59*, 2309−2312.
(24) Dhayal, R. S.; Liao, J.; Kahlal, S.; Wang, X.; Liu, Y.; Chiang, M.; van Zyl, W. E.; Saillard, J.; Liu, C. W. $[Cu_{32}(H)_{20}\{S_2P(O^iPr)_2\}_{12}]$: The Largest Number of Hydrides Recorded in a Molecular Nanocluster by Neutron Diffraction. *Chem. Eur. J.* **2015**, *21*, 8369−8374.
(25) Hou, Y.; Wang, Y.; Xu, T.; Wang, Z.; Tian, W.; Sun, D.; Yu, X.; Xing, P.; Shen, J.; Xin, X.; Hao, J. Synergistic Multiple Bonds Induced Dynamic Self-Assembly of Silver Nanoclusters into Lamellar Frameworks with Tailored Luminescence. *Chem. Mater.* **2022**, *34*, 8013−8021.
(26) Gunawardene, P. N.; Corrigan, J. F.; Workentin, M. S. Golden Opportunity: A Clickable Azide-Functionalized $[Au_{25}(SR)_{18}]^-$ Nanocluster Platform for Interfacial Surface Modifications. *J. Am. Chem. Soc.* **2019**, *141*, 11781−11785.
(27) Han, B.; Liu, Z.; Feng, L.; Wang, Z.; Gupta, R. K.; Aikens, C. M.; Tung, C.; Sun, D. Polymorphism in Atomically Precise Cu_{23} Nanocluster Incorporating Tetrahedral $[Cu_4]^0$ Kernel. *J. Am. Chem. Soc.* **2020**, *142*, 5834−5841.
(28) Li, Q.; Lambright, K. J.; Taylor, M. G.; Kirschbaum, K.; Luo, T.; Zhao, J.; Mpourmpakis, G.; Mokashi-Punekar, S.; Rosi, N. L.; Jin, R. Reconstructing the Surface of Gold Nanoclusters by Cadmium Doping. *J. Am. Chem. Soc.* **2017**, *139*, 17779−17782.
(29) Nguyen, T. D.; Jones, Z. R.; Goldsmith, B. R.; Buratto, W. R.; Wu, G.; Scott, S. L.; Hayton, T. W. A Cu_{25} Nanocluster with Partial Cu(0) Character. *J. Am. Chem. Soc.* **2015**, *137*, 13319−13324.
(30) Yonesato, K.; Ito, H.; Itakura, H.; Yokogawa, D.; Kikuchi, T.; Mizuno, N.; Yamaguchi, K.; Suzuki, K. Controlled Assembly Synthesis of Atomically Precise Ultrastable Silver Nanoclusters with Polyoxometalates. *J. Am. Chem. Soc.* **2019**, *141*, 19550−19554.
(31) Narouz, M. R.; Osten, K. M.; Unsworth, P. J.; Man, R. W. Y.; Salorinne, K.; Takano, S.; Tomihara, R.; Kaappa, S.; Malola, S.; Dinh, C. T.; Padmos, J. D.; Ayoo, K.; Garrett, P. J.; Nambo, M.; Horton, J. H.; Sargent, E. H.; Häkkinen, H.; Tsukuda, T.; Crudden, C. M. N-heterocyclic carbene-functionalized magic-number gold nanoclusters. *Nat. Chem.* **2019**, *11*, 419−425.
(32) Jadzinsky, P. D.; Calero, G.; Ackerson, C. J.; Bushnell, D. A.; Kornberg, R. D. Structure of a Thiol Monolayer-Protected Gold Nanoparticle at 1.1 Å Resolution. *Science* **2007**, *318*, 430−433.
(33) Cai, X.; Li, G.; Hu, W.; Zhu, Y. Catalytic Conversion of CO_2 over Atomically Precise Gold-Based Cluster Catalysts. *ACS Catal.* **2022**, *12*, 10638−10653.
(34) Liang, H.; Liu, B.; Tang, B.; Zhu, S.; Li, S.; Ge, X.; Li, J.; Zhu, J.; Xiao, F. Atomically Precise Metal Nanocluster-Mediated Photocatalysis. *ACS Catal.* **2022**, *12*, 4216−4226.
(35) Yoskamtorn, T.; Yamazoe, S.; Takahata, R.; Nishigaki, J.; Thivasasith, A.; Limtrakul, J.; Tsukuda, T. Thiolate-Mediated Selectivity Control in Aerobic Alcohol Oxidation by Porous Carbon-Supported Au_{25} Clusters. *ACS Catal.* **2014**, *4*, 3696−3700.
(36) Sun, C.; Mammen, N.; Kaappa, S.; Yuan, P.; Deng, G.; Zhao, C.; Yan, J.; Malola, S.; Honkala, K.; Häkkinen, H.; Teo, B. K.; Zheng, N. F. Atomically Precise, Thiolated Copper-Hydride Nanoclusters as Single-Site Hydrogenation Catalysts for Ketones in Mild Conditions. *ACS Nano* **2019**, *13*, 5975−5986.
(37) Dong, C.; Huang, R. W.; Sagadevan, A.; Yuan, P.; Gutiérrez-Arzaluz, L.; Ghosh, A.; Nematulloev, S.; Alamer, B.; Mohammed, O. F.; Hussain, I.; Rueping, M.; Bakr, O. M. Isostructural Nanocluster Manipulation Reveals Pivotal Role of One Surface Atom in Click Chemistry. *Angew. Chem., Int. Ed.* **2023**, *62*, e202307140.
(38) Guan, Z.; Li, J.; Hu, F.; Wang, Q. M. Structural Engineering toward Gold Nanocluster Catalysis. *Angew. Chem., Int. Ed.* **2022**, *61*, e202209725.
(39) Jin, L.; Weinberger, D. S.; Melaimi, M.; Moore, C. E.; Rheingold, A. L.; Bertrand, G. Trinuclear gold clusters supported by cyclic (alkyl)(amino)carbene ligands: mimics for gold heterogeneous catalysts. *Angew. Chem., Int. Ed.* **2014**, *53*, 9059−9063.
(40) Liu, L.; Wang, Z.; Wang, Z.; Wang, R.; Zang, S. Q.; Mak, T. C. W. Mediating CO_2 Electroreduction Activity and Selectivity over Atomically Precise Copper Clusters. *Angew. Chem., Int. Ed.* **2022**, *61*, e202205626.
(41) Qin, Z.; Sharma, S.; Wan, C.; Malola, S.; Xu, W.; Häkkinen, H.; Li, G. A Homoleptic Alkynyl-Ligated $[Au_{13}Ag_{16}L_{24}]^{3-}$ Cluster as a Catalytically Active Eight-Electron Superatom. *Angew. Chem., Int. Ed.* **2021**, *60*, 970−975.
(42) Shen, H.; Xu, Z.; Hazer, M. S. A.; Wu, Q.; Peng, J.; Qin, R.; Malola, S.; Teo, B. K.; Häkkinen, H.; Zheng, N. F. Surface Coordination of Multiple Ligands Endows N-Heterocyclic Carbene-Stabilized Gold Nanoclusters with High Robustness and Surface Reactivity. *Angew. Chem., Int. Ed.* **2021**, *60*, 3752−3758.
(43) Yang, D.; Pei, W.; Zhou, S.; Zhao, J.; Ding, W.; Zhu, Y. Controllable Conversion of CO_2 on Non-Metallic Gold Clusters. *Angew. Chem., Int. Ed.* **2020**, *59*, 1919−1924.
(44) Yonesato, K.; Yamazoe, S.; Yokogawa, D.; Yamaguchi, K.; Suzuki, K. A Molecular Hybrid of an Atomically Precise Silver Nanocluster and Polyoxometalates for H_2 Cleavage into Protons and Electrons. *Angew. Chem., Int. Ed.* **2021**, *60*, 16994−16998.
(45) Dong, J.; Robinson, J. R.; Gao, Z.; Wang, L. Selective Semihydrogenation of Polarized Alkynes by a Gold Hydride Nanocluster. *J. Am. Chem. Soc.* **2022**, *144*, 12501−12509.
(46) Gao, Z.; Wei, K.; Wu, T.; Dong, J.; Jiang, D.; Sun, S.; Wang, L. A Heteroleptic Gold Hydride Nanocluster for Efficient and Selective Electrocatalytic Reduction of CO_2 to CO. *J. Am. Chem. Soc.* **2022**, *144*, 5258−5262.
(47) Kulkarni, V. K.; Khiarak, B. N.; Takano, S.; Malola, S.; Albright, E. L.; Levchenko, T. I.; Aloisio, M. D.; Dinh, C. T.; Tsukuda, T.; Häkkinen, H.; Crudden, C. M. N-Heterocyclic Carbene-Stabilized Hydrido Au_{24} Nanoclusters: Synthesis, Structure, and Electrocatalytic Reduction of CO_2. *J. Am. Chem. Soc.* **2022**, *144*, 9000−9006.
(48) Li, G.; Jin, R. Gold Nanocluster-Catalyzed Semihydrogenation: A Unique Activation Pathway for Terminal Alkynes. *J. Am. Chem. Soc.* **2014**, *136*, 11347−11354.
(49) Tang, Q.; Lee, Y.; Li, D. Y.; Choi, W.; Liu, C. W.; Lee, D.; Jiang, D. Lattice-Hydride Mechanism in Electrocatalytic CO_2 Reduction by Structurally Precise Copper-Hydride Nanoclusters. *J. Am. Chem. Soc.* **2017**, *139*, 9728−9736.
(50) Kawawaki, T.; Mitomi, Y.; Nishi, N.; Kurosaki, R.; Oiwa, K.; Tanaka, T.; Hirase, H.; Miyajima, S.; Niihori, Y.; Osborn, D. J.; Koitaya, T.; Metha, G. F.; Yokoyama, T.; Iida, K.; Negishi, Y. Pt_{17} nanocluster electrocatalysts: preparation and origin of high oxygen reduction reaction activity. *Nanoscale* **2023**, *15*, 7272−7279.
(51) Xu, X.; Liu, Y.; Sun, F.; Jia, Y.; Xu, Q.; Tang, J.; Xie, Z.; Sun, J.; Li, S.; Tang, Q.; Guo, S.; Shen, H.; Zheng, N. F. Array-Based Clusters of Copper with Largely Exposed Metal Sites for Promoting Catalysis. *Chem. Mater.* **2023**, *35*, 7588−7596.
(52) Yao, Q.; Yuan, X.; Chen, T.; Leong, D. T.; Xie, J. Engineering Functional Metal Materials at the Atomic Level. *Adv. Mater.* **2018**, *30*, 1802751.
(53) Li, Q.; Zhou, D.; Chai, J.; So, W.; Cai, T.; Li, M.; Peteanu, L.; Chen, O.; Cotlet, M.; Wendy, G.; Zhu, H.; Jin, R. Structural distortion and electron redistribution in dual-emitting gold nanoclusters. *Nat. Commun.* **2020**, *11*, 2897.
(54) Sun, J.; Yan, X.; Wang, L.; Xie, Z.; Tian, G.; Wang, L.; He, A.; Li, S.; Guo, Q.; Chaolumen; He, J.; Shen, H. Decorating an Anticuboctahedral Copper Kernel with Labile Surface Coatings for Controlling Optical and Catalytic Properties. *Inorg. Chem.* **2023**, *62*, 9005−9013.

https://doi.org/10.1021/jacsau.4c00574
JACS Au 2024, 4, 3427−3435

(55) Li, Y.; Song, Y.; Zhang, X.; Liu, T.; Xu, T.; Wang, H.; Jiang, D.; Jin, R. Atomically Precise Au_{42} Nanorods with Longitudinal Excitons for an Intense Photothermal Effect. *J. Am. Chem. Soc.* **2022**, *144*, 12381−12389.
(56) Chen, T.; Yang, S.; Song, Y.; Chai, J.; Li, Q.; Ma, X.; Li, G.; Yu, H.; Zhu, M. All-thiolate-stabilized Ag_{42} nanocluster with a tetrahedral kernel and its transformation to an Ag_{61} nanocluster with a bi-tetrahedral kernel. *Chem. Commun.* **2020**, *56*, 7605−7608.
(57) Yuan, S. F.; Lei, Z.; Guan, Z.; Wang, Q. M. Atomically Precise Preorganization of Open Metal Sites on Gold Nanoclusters with High Catalytic Performance. *Angew. Chem., Int. Ed.* **2021**, *60*, 5225−5229.
(58) Baghdasaryan, A.; Bürgi, T. Copper nanoclusters: designed synthesis, structural diversity, and multiplatform applications. *Nanoscale* **2021**, *13*, 6283−6340.
(59) Sun, J.; Tang, X.; Liu, Z.; Xie, Z.; Yan, B.; Yin, R.; Chaolumen; Zhang, J.; Fang, W.; Wei, J.; Shen, H. Labile Ligands Protected Cu_{50} Nanoclusters with Tailorable Optical Limiting Effect. *ACS Mater. Lett.* **2024**, *6*, 281−289.
(60) Xu, C.; Jin, Y.; Fang, H.; Zheng, H.; Carozza, J.; Pan, Y.; Wei, P.; Zhang, Z.; Wei, Z.; Zhou, Z.; Han, H. A High-Nuclearity Copper Sulfide Nanocluster [S-Cu_{50}] Featuring a Double-Shell Structure Configuration with Cu(II)/Cu(I) Valences. *J. Am. Chem. Soc.* **2023**, *145*, 25673−25685.
(61) Biesinger, M.; Lau, L.; Gerson, A.; Smart, R. Resolving surface chemical states in XPS analysis of first row transition metals, oxides and hydroxides: Sc, Ti, V, Cu and Zn. *Appl. Surf. Sci.* **2010**, *257*, 887−898.
(62) Major, G.; Fairley, N.; Sherwood, P.; Linford, M.; Terry, J.; Fernandez, V.; Artyushkova, K. Practical guide for curve fitting in X-ray photoelectron spectroscopy. *J. Vac. Sci. Technol. A* **2020**, *38*, 061203.
(63) Yuan, P.; Chen, R.; Zhang, X.; Chen, F.; Yan, J.; Sun, C.; Ou, D.; Peng, J.; Lin, S.; Tang, Z.; Teo, B. K.; Zheng, L.; Zheng, N. F. Ether-Soluble Cu_{53} Nanoclusters as an Effective Precursor of High-Quality CuI Films for Optoelectronic Applications. *Angew. Chem., Int. Ed.* **2019**, *58*, 835−839.
(64) Yuan, X.; Sun, C.; Li, X.; Malola, S.; Teo, B. K.; Häkkinen, H.; Zheng, L.; Zheng, N. F. Combinatorial Identification of Hydrides in a Ligated Ag_{40} Nanocluster with Noncompact Metal Core. *J. Am. Chem. Soc.* **2019**, *141*, 11905−11911.
(65) Liao, J.; Brocha Silalahi, R. P.; Chiu, T.; Liu, C. W. Locating Interstitial Hydrides in $MH_2@Cu_{14}$ (M = Cu, Ag) Clusters by Single-Crystal X-ray Diffraction. *ACS Omega* **2023**, *8*, 31541−31547.
(66) Huang, R. W.; Yin, J.; Dong, C.; Maity, P.; Hedhili, M. N.; Nematulloev, S.; Alamer, B.; Ghosh, A.; Mohammed, O. F.; Bakr, O. M. $[Cu_{23}(PhSe)_{16}(Ph_3P)_8(H)_6]\cdot BF_4$: Atomic-Level Insights into Cuboidal Polyhydrido Copper Nanoclusters and Their Quasi-simple Cubic Self-Assembly. *ACS Materials Lett.* **2021**, *3*, 90−99.
(67) Ha, J. M.; Solovyov, A.; Katz, A. Synthesis and Characterization of Accessible Metal Surfaces in Calixarene-Bound Gold Nanoparticles. *Langmuir* **2009**, *25*, 10548−10553.
(68) de Silva, N.; Ha, J. M.; Solovyov, A.; Nigra, M. M.; Ogino, I.; Yeh, S. W.; Durkin, K. A.; Katz, A. A bioinspired approach for controlling accessibility in calix[4]arene-bound metal cluster catalysts. *Nat. Chem.* **2010**, *2*, 1062−1068.
(69) Xu, J.; Zhao, F.; Yuan, Y.; Wu, X. Ruthenium-Catalyzed Carbonylative Coupling of Anilines with Organoboranes by the Cleavage of Neutral Aryl C-N Bond. *Org. Lett.* **2020**, *22*, 2756−2760.
(70) Usman, M.; Ren, Z.; Wang, Y.; Guan, Z. Copper-catalyzed carbonylation of anilines by diisopropyl azodicarboxylate for the synthesis of carbamates. *RSC Adv.* **2016**, *6*, 107542−107546.

https://doi.org/10.1021/jacsau.4c00574
JACS Au 2024, 4, 3427−3435